EBioMedicine 2 (2015) 135–146

Contents lists available at ScienceDirect

EBioMedicine

journal homepage: www.ebiomedicine.com

Rare Autism-Associated Variants Implicate Syntaxin 1 (STX1 R26Q) Phosphorylation and the Dopamine Transporter (hDAT R51W) in Dopamine Neurotransmission and Behaviors

Etienne Cartier [a,1], Peter J. Hamilton [b,c,1], Andrea N. Belovich [d], Aparna Shekar [d], Nicholas G. Campbell [b], Christine Saunders [d], Thorvald F. Andreassen [e], Ulrik Gether [e], Jeremy Veenstra-Vanderweele [f], James S. Sutcliffe [b,g], Paula G. Ulery-Reynolds [h], Kevin Erreger [a,c,*,2], Heinrich J.G. Matthies [a,c,*,2], Aurelio Galli [a,b,c,d,*,2]

[a] Department of Molecular Physiology & Biophysics, Vanderbilt University School of Medicine, Nashville, TN 37232-8548, United States
[b] Vanderbilt Brain Institute, Vanderbilt University School of Medicine, Nashville, TN 37232-8548, United States
[c] Neuroscience Program in Substance Abuse, Vanderbilt University School of Medicine, Nashville, TN 37232-8548, United States
[d] Department of Pharmacology, Vanderbilt University School of Medicine, Nashville, TN 37232-8548, United States
[e] Molecular Neuropharmacology and Genetics Laboratory, Department of Neuroscience and Pharmacology, Faculty of Health and Medical Sciences, University of Copenhagen, DK-2200 Copenhagen, Denmark
[f] Department of Psychiatry and New York State Psychiatric Institute, Columbia University, New York, NY 10032, United States
[g] Department of Psychiatry, Vanderbilt University School of Medicine, Nashville, TN 37232-8548, United States
[h] Department of Psychiatry, UT Southwestern Medical Center, Dallas, TX 75390-8813, United States.

ARTICLE INFO

Article history:
Received 11 December 2014
Received in revised form 13 January 2015
Accepted 15 January 2015
Available online 16 January 2015

Keywords:
Autism spectrum disorder
Dopamine
Transporter
Drosophila
Syntaxin 1
Casein kinase 2

ABSTRACT

Background: Syntaxin 1 (STX1) is a presynaptic plasma membrane protein that coordinates synaptic vesicle fusion. STX1 also regulates the function of neurotransmitter transporters, including the dopamine (DA) transporter (DAT). The DAT is a membrane protein that controls DA homeostasis through the high-affinity re-uptake of synaptically released DA.
Methods: We adopt newly developed animal models and state-of-the-art biophysical techniques to determine the contribution of the identified gene variants to impairments in DA neurotransmission observed in autism spectrum disorder (ASD).
Outcomes: Here, we characterize two independent autism-associated variants in the genes that encode STX1 and the DAT. We demonstrate that each variant dramatically alters DAT function. We identify molecular mechanisms that converge to inhibit reverse transport of DA and DA-associated behaviors. These mechanisms involve decreased phosphorylation of STX1 at Ser14 mediated by casein kinase 2 as well as a reduction in STX1/DAT interaction. These findings point to STX1/DAT interactions and STX1 phosphorylation as key regulators of DA homeostasis.
Interpretation: We determine the molecular identity and the impact of these variants with the intent of defining DA dysfunction and associated behaviors as possible complications of ASD.

1. Introduction

Autism spectrum disorder (ASD) is defined by deficits in social communication and by the presence of restricted and repetitive behaviors, which are often the first signs of ASD (Rowberry et al., 2015; Wolff et al., 2014). Increased striatal size is among the most consistent neuroimaging findings in ASD, and increased size and growth of the striatum, a dopamine (DA) enriched brain region, have been associated with severity of repetitive behaviors (Langen et al., 2007, 2009, 2014; Hollander et al., 2005). Consistent with the involvement of striatal dysfunction in ASD, recent studies have found that individuals with ASD display diminished response to reward (Dichter et al., 2012; Damiano et al., 2012; Lin et al., 2012) which stems from striatal hypofunction (Kohls et al., 2013, 2014). Striatal DA input has important roles in reward, movement, and habit (Zald et al., 2004; Howe et al., 2011, 2013). Importantly, excessive striatal

* Corresponding authors at: Room 7124, MRB III, Vanderbilt University School of Medicine, 465 21st Avenue South, Nashville, TN 37232-8548, United States.
E-mail addresses: kevin.erreger@vanderbilt.edu (K. Erreger), heinrich.j.matthies@vanderbilt.edu (H.J.G. Matthies), aurelio.galli@vanderbilt.edu (A. Galli).
[1] E.C. and P.J.H. contributed equally to this work.
[2] H.J.G.M., K.E., and A.G. contributed equally to this work.

http://dx.doi.org/10.1016/j.ebiom.2015.01.007

dopaminergic signaling results in repetitive behavior (Fasano and Petrovic, 2010).

The DA transporter (DAT) shapes striatal DA signaling via re-uptake of synaptically released DA (Kristensen et al., 2011). In addition to its role in vesicular fusion, the plasma membrane protein syntaxin 1 (STX1) plays a pivotal role in regulating DAT functions (Binda et al., 2008), and it has been observed to regulate other neurotransmitters: sodium symporters (NSS) (Quick, 2002, 2003, 2006; Dipace et al., 2007). Therefore, at the dopaminergic synapse, in addition to synaptic release, the actions of STX1 may regulate DAT functions and, as a consequence, DA neurotransmission and associated behaviors.

ASD is associated with variants in several genes of the DA network, including those encoding STX1 (Nakamura et al., 2008, 2011; Durdiakova et al., 2014), the DAT (Hamilton et al., 2013; Bowton et al., 2014), DA receptors, as well as enzymes involved in DA metabolism (Hettinger et al., 2012; Qian et al., 2013; Reiersen and Todorov, 2011; Yoo et al., 2013; Nguyen et al., 2014). Altered gene expression of *STX1A* has also been described in post-mortem brain and in lymphocytes from people with ASD (Nakamura et al., 2008, 2011). These data point to DA dysfunction as a potential complication and possible risk factor for ASD, but without a clear understanding of the underlying mechanisms.

Here, we have identified rare, inherited, functional missense variants in the gene that encodes STX1 (*STX1A*; resulting in an Arg to Gln substitution at site 26) and in the gene that encodes DAT (*SLC6A3*; resulting in an Arg to Trp substitution at site 51) in separate individuals with ASD. Among the different DAT functions, reverse transport of DA has emerged as a contributing factor in DA neurotransmission and remains incompletely understood (Leviel, 2011). Both of these variants disrupt the molecular mechanisms of reverse transport of DA, resulting in DA dysfunction and associated behavioral abnormalities. To mechanistically characterize these variants, we identify novel molecular events involved in the STX1 regulation of DAT. Our results suggest a coordinated molecular network, including STX1 and DAT that might contribute to disruption of dopaminergic signaling in individual with ASD.

2. Materials and Methods

All human subjects provided informed consent and the research was approved by institutional human subjects boards. All experiments, procedures, and surgeries involving mice were performed in compliance with and were approved by the Institutional Animal Care and Use Committee of Vanderbilt University.

2.1. Subjects and Clinical Assessment

All ASD cases were ascertained using the Autism Diagnostic Interview—Revised (ADIR), the Autism Diagnostic Observation Schedule—Generic (ADOS), and the DSM-IV diagnosis of pervasive developmental disorder (Neale et al., 2012; Lim et al., 2013; Liu et al., 2013). Clinical assessment of families harboring either variant is dependent on which collection they belong to. In brief, families that contain the *SLC6A3* R/W or *STX1A* R/Q variant belong to the Autism Sequencing Consortium (ASC) and the Simons Simplex Collection (SSC) respectively, and have been previously reported (Neale et al., 2012; De Rubeis et al., 2014; Iossifov et al., 2014).

ADIR is an extensive, semi-structured parent/guardian interview that queries both historical and current information on the development, behavior, and skills of a child. The ADOS is a structured observational assessment administered directly to participants. It is employed to confirm behaviors reported on the ADIR and consists of modules adapted for differing language abilities. When used together, the ADIR and ADOS are deemed the “gold-standard” instruments for validating and ASD diagnosis.

2.2. SLC6A3 R/W and STX1A R/Q Discovery and Validation

Methodological details on *SLC6A3* R/W and *STX1A* R/Q discovery are published (Neale et al., 2012; De Rubeis et al., 2014; Iossifov et al., 2014) and validation of the variant was performed as described in Bowton et al. (2014). DNA derived from both parents, the probands, and siblings were subjected to sequence analysis. In all instances, each variant was predicted to be heterozygous at their respective site and experimentally validated and confirmed via Sanger sequencing.

2.3. Cell Culture and Transfection

STX1 constructs in the pcDNA3.1(−) expression vector and the GFP-hDAT-pCIHygro expression vectors containing hDAT or hDAT R/W (Arg51 to Trp) sequence were generated, confirmed and transiently transfected into Chinese hamster ovary (CHO) cells. In some experiments (noted in figure legend), stably transfected hDAT CHO cells were used. These cells were generated as described in Bowton et al. (2010). Cells were maintained in a 5% CO_2 incubator at 37 °C and maintained in Ham's F-12 medium supplemented with 10% fetal bovine serum (FBS), 1 mM L-glutamine, 100 U/mL penicillin, and 100 μg/mL streptomycin. Stably transfected hDAT CHO cells were kept under selection with 250 μg/mL hygromycin B (Corning Cellgro). Fugene-6 (Roche Molecular Biochemicals) in serum-free media was used to transfect cells using a 6:1 transfection reagent:DNA ratio. Assays were conducted 24–48 h post-transfection.

2.4. Superior Cervical Ganglion Neuron Culture and Transfection

SCG neurons were cultured from 1 to 3 day old male mouse pups. SCGs were dissected in complete Ultraculture medium (Lonza) supplemented with 20 ng/mL nerve growth factor (NGF). SCGs were washed with PBS and incubated for 20 min in collagenase (3%) and trypsin (2.5%) at 37 °C. They were washed in complete Ultraculture medium with NGF. Dissociated cells were obtained by SCG trituration in medium. Cells were plated on poly-D-lysine coated MatTek® dish treated with collagen (type IV). 24 h post-plating, the media was replaced with Ultraculture medium with NGF and 10 μM 5-fluoro-2-deoxyuridine (FDU). SCGs were transfected via intranuclear microinjection of DNA.

2.5. Cell Surface Biotinylation and Protein Immunoblot

Cells were cultured in 6-well plates. For cell surface biotinylation assays, cells were labeled with sulfo-NHS-SS-biotin (1.0 mg/mL; Pierce) before purification and analysis via SDS-PAGE/immunoblots. hDAT was detected using a rat monoclonal primary antibody to the N-terminus of hDAT (1:1000) (Millipore Bioscience Research Reagents, catalog number MAB369) and a goat-anti-rat-HRP-conjugated secondary antibody (1:5000) (Jackson ImmunoResearch, catalog number sc-2006). The phosphorylation level of STX1 at Ser14 was detected using a rabbit polyclonal antibody against phospho-S14 either from Castillo et al. (2010) or with a commercially available antibody (1:2500) (Abcam, catalog number ab63571) and with a goat-anti-rabbit-HRP-conjugated secondary antibody (1:5000) (Jackson ImmunoResearch, catalog number sc-3837). Total STX1 was detected using a mouse monoclonal antibody (1:5000) (Sigma, catalog number S 0664) and a goat-anti-mouse-HRP-conjugated secondary antibody (1:5000) (Jackson ImmunoResearch, catalog number sc-2005).

2.6. Immunostaining

SCG neurons (at least 14 days in culture) were serum starved for 1 h in DMEM:F12 and treated with vehicle or AMPH for 20 min. Neurons were subsequently fixed with PBS plus Ca^{2+}/Mg^{2+} and 4% paraformaldehyde, washed three times with PBS plus Ca^{2+}/Mg^{2+}, permeabilized and blocked with PBS with 4% bovine serum albumin (BSA)/0.15%

Tween 20, and immunostained with the appropriate antibody dissolved in PBS plus 4% BSA and 0.05% Tween 20. NET was detected using a mouse monoclonal antibody (1:5000) (Mab Technologies; NET05-2) and p-STX1 with an affinity purified rabbit polyclonal (1:1000), anti-pSTX at Ser14 (Castillo et al., 2010). Primary antibodies were visualized with the appropriate Alexa-labeled secondary antibody from Invitrogen.

Mouse brain slices were prepared as outlined in the High Speed Chronoamperometry section, except recovery was in aCSF for 1 h at 37 °C. Slices were fixed, permeabilized, washed, and blocked as outlined above. DAT was visualized using rat monoclonal against DAT and STX1A and STX1B were detected using rabbit polyclonal antiserum from SYSY. p-STX at Ser14 was detected using an affinity purified rabbit polyclonal(1:1000) (Castillo et al., 2010). Primary antibodies were visualized with the appropriate covalently Alexa-labeled secondary antibody from Invitrogen.

Immunofluorescence was imaged by capturing Z-series using a 63× Plan-APOCHROMAT oil lens (Vanderbilt University Medical Center Cell Imaging Shared Resource). All images shown are from single confocal sections, and image processing was performed using ImageJ and Adobe Photoshop.

2.7. Co-immunoprecipitations

Cells were grown to confluence in 25 cm^2 culture flasks and serum deprived for 1 h prior to assay. Cells were washed three times with 4 °C phosphate-buffered saline (Gibco) containing 1 mM EGTA and 1 mM EDTA, and then lysed in RIPA buffer (100 mM NaCl, 1.0% IGEPAL CA-630 (NP-40), 0.5% sodium deoxycholate, 0.1% SDS, 50 mM Tris, pH = 7.4, supplemented with a protease inhibitor cocktail (Sigma)). Lysates were passed twice through a 27.5 gauge needle, and centrifuged at 15,000 ×*g* for 30 min. With a portion of the total cell lysate (TCL) collected to run as the totals, 1 mL of the remaining supernatant was incubated at 4 °C for 4 h with Sepharose-G beads (Fisher Scientific), previously washed with 1% BSA in RIPA buffer, and then preincubated with 2.5 μg DAT antibody (rat monoclonal, #MAB369, Millipore). For the control, supernatant was incubated with BSA-blocked Sepharose-G beads alone (no DAT antibody). After the 4-hour incubation, beads were spun down, washed with cold RIPA buffer, and eluted with Laemmli sample buffer at 37 °C for 30 min. TCL and bead eluates were analyzed by SDS-PAGE (10%) and immunoblotted for total STX1 and DAT. Band intensity was quantified using ImageJ software (National Institutes of Health).

2.8. Expression and Purification of STX1

The cDNAs encoding STX, STX S14D and STX S14A lacking the transmembrane domain (STXΔTM, STX1ΔTM S14A and STX1ΔTM S14D) were inserted into the bacterial expression vector pGEX, thereby adding an N-terminal GST-tag followed by a thrombin cleavage site. The resulting fusion proteins were produced in *Escherichia coli* BL21 DE3 LysS. The culture was grown at 30 °C to OD 0.8 and expression was induced with 1 mM isopropylβ-D-1-thiogalactopyranoside at 30 °C, and the culture was harvested 4 h after induction. The frozen pelleted bacteria were lyzed in buffer (PBS, 0.1% TX-100, 20 μg/mL DNAse I, 1 mM DTT, mix protease inhibitor (GE Healthcare)). The lysate was cleared by centrifugation followed by incubation with 100 μL glutathione sepharose beads (GE Healthcare, Uppsala, Sweden) at 4 °C for 1.5 h. The beads were pelleted at 3000 rpm for 5 min and washed 3 times in buffer (PBS, 0.1% TX-100, 1 mM DTT) before elution by cleavage with 1 μL thrombin (GE Healthcare, Uppsala, Sweden) O/N at 4 °C. PMSF (1 mM) was added, and the beads were filtered through a P200 tip. The concentration of the purified STX1B was measured by BCA assay (Thermo Fisher Scientific, Waltham, MA).

2.9. GST Pull-Down Assay

A DAT GST fusion protein containing the 64 N-terminal residues of the transporter (GST hDAT 1–64) was expressed and bound to glutathione sepharose beads as described (Binda et al., 2008). For the pull-down, 20 μL beads with either GST or GST hDAT 1–64 bound were incubated with 2 μg of purified STXΔTM, STX1ΔTM S14A or STX1ΔTM S14D in 500 μL buffer (PBS, 0.1% TX-100, 0.1% BSA) for 30 min at 4 °C and washed three times in buffer without BSA. Bound protein was eluted by incubation of beads for 1 h at room temperature with 1 μL thrombin in 15 μL buffer (PBS, 0.1% TX-100) followed by addition of SDS loading buffer + 100 mM DTT and incubation for 25 min at 70 °C. Each sample was split in two and loaded in two different Any-kD precast gels (BioRad, Hercules, CA). One gel was used as a Coomassie loading control and the other was transfered to a PDVF membrane and immunoblotted with primary mouse STX1 antibody (Sigma Aldrich. St. Louis, MO) 1:1000 and anti-mouse HRP-conjugated secondary antibody (Thermo Fisher Scientific, Waltham, MA) 1:5000.

2.10. Amperometry

Cells were plated at a density of ~20,000 per 35-mm culture dish. To load cells with DA, dishes were washed with KRH assay buffer (130 mM NaCl, 1.3 mM KCl, 1.2 mM KH_2PO_4, 10 mM HEPES, and 2.2 mM $CaCl_2$, pH 7.4) containing 10 mM dextrose, 100 μM pargyline, 1 mM tropolone, and 100 μM ascorbic acid, and incubated with 1 μM DA in KRH assay buffer for 20 min at 37 °C. To preload SCG neurons, dishes were washed with KRH assay buffer (as above) containing 100 nM raclopride. Dishes were washed three times with the external bath solution (130 mM NaCl, 10 mM HEPES, 34 mM dextrose, 1.5 mM $CaCl_2$, 0.5 mM $MgSO_4$, 1.3 mM KH_2PO_4, adjusted pH to 7.35, and 300 mOsm). A carbon fiber electrode (ProCFE; fiber diameter of 5 μm; obtained from Dagan Corporation) juxtaposed to the plasma membrane and held at +700 mV (a potential greater than the oxidation potential of DA) was used to measure DA flux through oxidation reactions. Amperometric currents in response to the addition of 10 μM AMPH were recorded using an Axopatch 200B amplifier (Molecular Devices, Union City, CA) with a low-pass Bessel filter set at 1 kHz; traces were digitally filtered offline at 1 Hz using Clampex9 software (Molecular Devices, Union City, CA). DA efflux was quantified as the peak value of the amperometric current for all experiments except for recordings from SCG neurons. For SCG neurons, total DA efflux was quantified as the integral of the trace for a fixed 15-minute window.

2.11. High Speed Chronoamperometry

Striatal hemislices (300 μm) from 6 to 10 week old C57BL/6 mice were prepared with a vibratome (Leica VT1000S) in an ice cold oxygenated (95% O2/5% CO_2) sucrose cutting solution consisting of (in mM): 210 sucrose, 20 NaCl, 2.5 KCl, 1 $MgCl_2$, 1.2 NaH_2PO_4, 10 glucose, 26 $NaHCO_3$. Slices were then transferred to oxygenated artificial cerebrospinal fluid (aCSF) at 28 °C for a minimum of 1 h. The aCSF consisted of (in mM): 125 NaCl, 2.5 KCl, 1 $MgCl_2$, 2 $CaCl_2$, 1.2 NaH_2PO_4, 10 glucose, 26 $NaHCO_3$, 0.25 ascorbic acid. Striatal slices were treated at 37 °C for 1 h with either 100 nM BONT/C or vehicle control. DA concentration was measured by chronoamperometry in striatal slices. Briefly, carbon fiber electrodes (100 μm length × 30 μm O.D.) coated with nafion for DA selectivity were lowered into the desired recording site or sites so that the tip of the recording electrode was positioned at a depth of 75–100 μm. The voltage was stepped from 0 mV to 550 mV for 100 ms and then back to 0 mV and the charging current of the carbon fiber electrode was allowed to decay for 20 msec before the signals were integrated. Data were collected at a frequency of 1 Hz with an Axopatch 200B amplifier. The integrated charge was converted to DA concentration based on in vitro calibration with DA.

2.12. [^{3}H]DA Uptake

For DA uptake in a heterologous expression system: cells were plated on poly-D-lysine coated, 24-well plates and grown to ~90% confluence. On the day of the experiment, cells were washed with 37 °C KRH buffer containing 10 mM dextrose, 100 μM pargyline, 1 mM tropolone, and 100 μM ascorbic acid, and equilibrated for 5 min at 37 °C. Saturation kinetics of DA uptake was determined using a mixture of [^{3}H]DA (PerkinElmer Life Sciences, Waltham, MA) and unlabeled DA (Sigma Aldrich) diluting to final DA concentrations of 0.05 μM–10 μM. Uptake was initiated by bath addition of the dilution row mixture. Uptake was terminated after 10 min by washing twice in ice-cold KRH buffer. Scintillation fluid (Optiphase HiSafe 3, PerkinElmer Life Sciences) was added to the wells and the plates were counted in a Wallac Tri-Lux β-scintillation counter (Wallac). Nonspecific binding was determined in the presence of 10 μM cocaine. K_m and V_{max} values were derived by fitting Michaelis–Menten kinetics to the background corrected uptake data, using GraphPad Prism 5.0 (GraphPad Software, San Diego, CA). All determinations were performed in triplicates.

For DA uptake in striatal slices: striatal hemislices (prepared as previously mentioned) were treated at 37 °C for 1 h with either 100 nM BONT/C or vehicle control. Slices were then exposed to 50 nM [^{3}H]DA for 10 min. DAT-specific DA uptake was determined by subtracting the non-specific signal in the presence of 3 μM GBR12909. At the end of the [^{3}H]DA treatment, the slices were washed with cold aCSF and the striatum dissected. Tissue samples were then homogenized in 200 μL of lysis buffer consisting of 150 mM NaCl, 25 mM HEPES, 2 mM sodium orthovanadate, 2 mM sodium fluoride, 1% Triton-100. The homogenate was centrifuged at 13,000 ×*g* at 4 °C for 30 min and the supernatant added to 500 μL of buffer 150 mM NaCl, 25 mM HEPES, 2 mM sodium orthovanadate, 2 mM sodium fluoride, 0.1% Triton-100. The protein concentration of each sample was measured and 500 μL of each sample was added to scintillation vials to count [^{3}H]DA. Counts were expressed as a ratio to protein content and normalized to the mean value for the control condition within each experiment.

For DA uptake in dissected *Drosophila* brains: 2–5 day old males were collected, anesthetized with CO_2, and brains were dissected in Schneider's medium (GIBCO) with 1.5% BSA. The retina was removed, and four brains per condition were pooled in Millipore Millicell inserts in 24 well plates. Brains were washed with Schneider's medium, then washed in a standard fly saline solution (HL3) plus 1.5% BSA and 10 mM $MgSO_4$. For 15 min at room temperature, brains were exposed to 200 nM [^{3}H]DA in HL3 plus 1.5% BSA and 115 μM ascorbic acid. Brains were then washed six times with 1.4 mL HL3 plus 1.5% BSA at 4 °C. Brains were placed into scintillation vials in 100 μL 0.1% SDS. Scintillation fluid was added to count [^{3}H]DA.

2.13. Drosophila Genetics, Molecular Biology, and Construction of UAS hDAT

Flies lacking the *Drosophila* dopamine transporter (*DAT^{fmn}*) (Kume et al., 2005) and flies harboring TH-Gal4 were outcrossed to a control line (Bloomington Indiana (BI) 6326) and selected by PCR or by eye color. TH-GAL4 (Bl 8848) and M{vas-int.Dm}ZH-2A, M{3xP3-RFP.attP′} ZH-22A (Bl 24481) were obtained from the BI stock center and outcrossed to flies lacking the *Drosophila* DAT (*DAT^{fmn}*) and carrying the *white* (*w^{1118}*) mutation (BI stock number 6236) for 5–10 generations. Transgenes (hDAT or hDAT R/W) were cloned into pBI-UASC, and constructs were injected into embryos from M{vas-int.Dm}ZH-2A, M{3xP3-RFP.attP′}ZH-22A (Bl 24481). Initial potential transformants were isolated by selecting for red eyes and lack of GFP signal in the head. Transformants were also verified by RFP fluorescence and outcrossed 5–8 times to *DAT^{fmn}* flies. The presence of *DAT^{fmn}* lesion was verified by PCR. To generate CK2-DN flies, we drove the expression of a severely functionally compromised dominant negative version of CK2α (UAS-*Tik*) (Bose et al., 2006) in dopaminergic neurons by using TH-Gal4. UAS-*Tik* is based on a CK2α allele (*Tik*) that in a heterozygous condition, causes no obvious neural abnormalities (Lin et al., 2002). *Tik* has two substitutions, M161K and E165D. M161K is in the ATP-binding pocket preventing nucleotide-binding thereby eliminating catalytic activity (Lin et al., 2002; Rasmussen et al., 2005). Overexpression from the UAS-*Tik* construct to dominantly blocks CK2 function (Bose et al., 2006). Therefore, UAS-*Tik* can be used as a CK2-DN construct. Flies were maintained on a standard cornmeal/molasses/yeast media at 25 °C and 65% humidity with a 12 hour/12 hour light/dark cycle. Lights came on at 8 AM and off at 8 PM.

2.14. Behavioral Analysis

Three day old males were collected and placed into tubes with food for three days. After three days locomotion was recorded for 32 h by beam breaks and analyzed using equipment/software from Trikinetics (www.trikinetics.com). For the AMPH-induced locomotion, males were starved for 6 h and then fed sucrose (10 mM) containing either AMPH (1 mM) or vehicle.

2.15. Statistical Analysis

Compiled data are expressed as normalized mean ± s.e.m. For statistical analysis, we used either a Student's t-test or ANOVA depending on the n of the experimental groups. $p < 0.05$ was considered statistically significant.

3. Results

3.1. Autism-Related hDAT and STX1 Variants Alter DA Transport

Exome capture and sequencing analysis identified two families harboring separate rare and inherited SNPs. One family harbors a single nucleotide variant (SNV) in the gene that encodes hDAT (*SLC6A3*; resulting in an Arg to Trp substitution at site 51; hDAT R/W) (Fig. 1A, left panel). The other family harbors a SNV in the gene that encodes STX1A (*STX1A*; resulting in an Arg to Gln substitution at site 26; STX1 R/Q) (Fig. 1A, right panel). Neither of these SNVs were found in control samples (n = 1463) and were not deposited in the NHLBI Exome Sequencing Project (URL: http://evs.gs.washington.edu/EVS/) [3 (November, 2014) accessed].

The family harboring the *STX1A* R/Q variant is in a cohort of families belonging to the Simons Simplex Collection (SSC), a well-characterized ASD collection. The family harboring the *SLC6A3* R/W variant is in the cohort of families studied by the Autism Sequencing Consortium (ASC). Details on ASC samples and characteristics have been previously published (Neale et al., 2012). The ADIR scores are presented in table format in supplemental materials (Supp. Table 1). Thus, we are classifying these variants as ASD-specific. The hDAT Arg51 is located at the N-terminus in a region highly conserved across multiple species (Fig. 1B). STX1A Arg26 is located at the N-terminus and is also conserved across several species as well as in other STX1 isoforms, including STX1B (Fig. 1C). The two redundant neuronaThil STX1 isoforms (STX1A and STX1B) are 84% identical. Both isoforms are present in DA neurons and striatal DA terminals and colocalize with DAT (Supp. Fig. 1). In this study we utilize STX1B, here simply referred as STX1.

To evaluate whether the STX1 R/Q variant promotes DA dysfunction, we determined the impact of this variant on a key STX1 regulatory site (Ser14) implicated in neuropsychiatric disorders (Castillo et al., 2010) and hDAT function. hDAT cells (see Methods) expressing STX1 R/Q show reduced STX1 phosphorylation at Ser14 (Fig. 2A). One function of STX1 is to regulate the DAT-mediated reverse transport of DA in response to AMPH (Binda et al., 2008). Therefore, we used AMPH as a tool to probe whether STX1 R/Q has an altered ability to regulate DA efflux, measured by amperometry in hDAT cells. The amperometric probe, a carbon fiber electrode juxtaposed to the cell membrane,

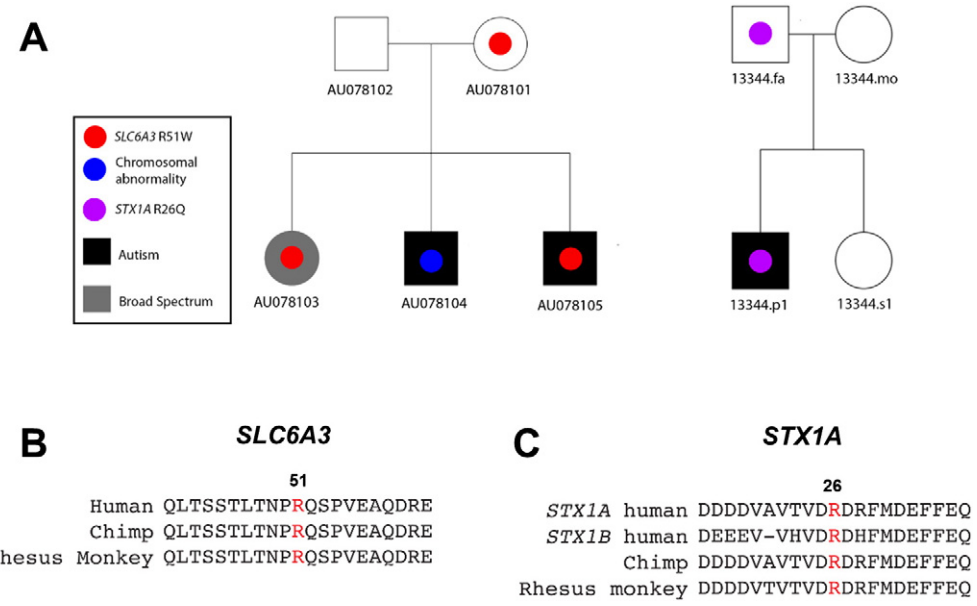

Fig. 1. Pedigree and cross-species conservation of hDAT R/W and STX1 R/Q. (A) Variant inheritance is shown for the families harboring the hDAT R/W and the STX1 R/Q genotypes. Filled symbols indicate individuals with an ASD diagnosis, while open symbols reflect individuals without an ASD diagnosis. (B) Alignment of the DAT amino acid sequence across multiple species. Arginine 51 is represented in red. (C) Alignment of the STX1 amino acid sequence across isoforms and multiple species. Arginine 25 is represented in red.

measures DA efflux by oxidation/reduction reactions, with DA efflux represented as a positive current. hDAT cells expressing STX1 R/Q display a significantly reduced AMPH-induced DA efflux as compared to hDAT cells expressing STX1 (Fig. 2B). It is important to point out that in hDAT cells expressing STX1 R/Q, the V_{max} of DA uptake was significantly increased, whereas the K_m of DA was not significantly different from that of hDAT cells expressing STX1 (Fig. 2C, top). A representative plot of DA uptake kinetics is shown in Fig. 2C (bottom). These data indicate that the STX1 R/Q variant asymmetrically regulates hDAT function by selectively impairing DA efflux.

In order to determine whether other ASD-associated variants can disrupt DAT function by parallel mechanisms to those of STX1, we explored changes in hDAT function in cells expressing hDAT R/W. The AMPH-induced reverse transport of DA was reduced in hDAT R/W cells with respect to hDAT cells (Fig. 3A). These data parallel the reduction in DA efflux observed in hDAT cells expressing the STX1 R/Q variant (Fig. 2B). This reduction in AMPH-induced DA efflux in the hDAT R/W is not mirrored by a significant reduction in DA uptake or DA apparent affinity (Fig. 3B), indicating the hDAT R/W variant also asymmetrically regulates hDAT function by selectively impairing DA efflux.

Previously, we determined that reverse transport of DA induced by AMPH is tightly regulated by the interaction of STX1 at the DAT N-terminus (Binda et al., 2008). Therefore, we explored whether the reduced reverse transport of DA in hDAT R/W cells stemmed from a

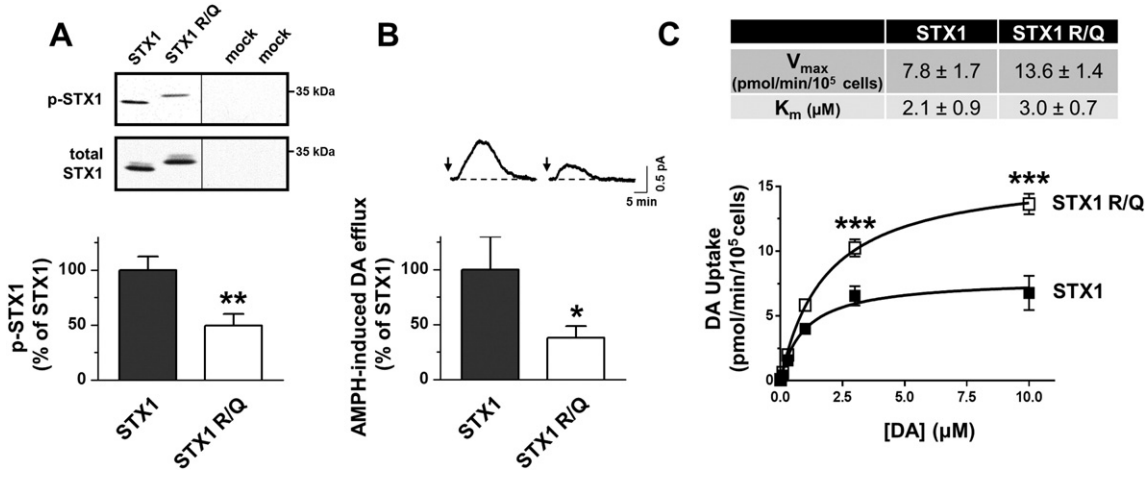

Fig. 2. STX1 R to Q missense variant decreases STX1 phosphorylation and reverse transport of DA without decreasing DA uptake: (A) Top: stably transfected hDAT cells expressing either STX1 or STX1 R/Q were immunoblotted with a phospho-specific antibody directed against STX1 at Ser14 (top lane). The mock transfection of GFP alone (mock) supports the absence of non-specific binding. Bottom lane shows total STX1 proteins. Bottom: quantitation of band intensities of phospho-STX1 (p-STX1) normalized to the respective total STX1 and expressed as a percentage STX1 (** = $p < 0.01$ by Student's t-test; n = 5, in triplicate). (B) Top: representative AMPH-induced DA efflux recorded from stably transfected hDAT cells expressing either STX1 or STX1 R/Q. Arrows indicate application of 10 μM AMPH. Bottom: quantitation of AMPH-induced DA efflux. Data are represented as maximal amperometric current expressed as percent of the current recorded in hDAT cells expressing STX1 (* = $p < 0.05$ by Student's t-test; n = 7). (C) STX1 R/Q enhances DAT-mediated DA uptake. Top: kinetic parameters (V_{max} and K_m) for stably transfected hDAT cells expressing either STX1 or STX1 R/Q (V_{max}: $p < 0.05$ by Student's t-test; n = 3, in triplicate; K_m: $p > 0.46$ by Student's t-test; n = 3, in triplicate). Bottom: representative plot of [^{3}H]DA uptake kinetics in stably transfected hDAT cells expressing STX1 (filled squares) and STX1 R/Q (empty squares) cells (*** = $p < 0.001$, by two-way ANOVA followed by Bonferroni post-test; in triplicate).

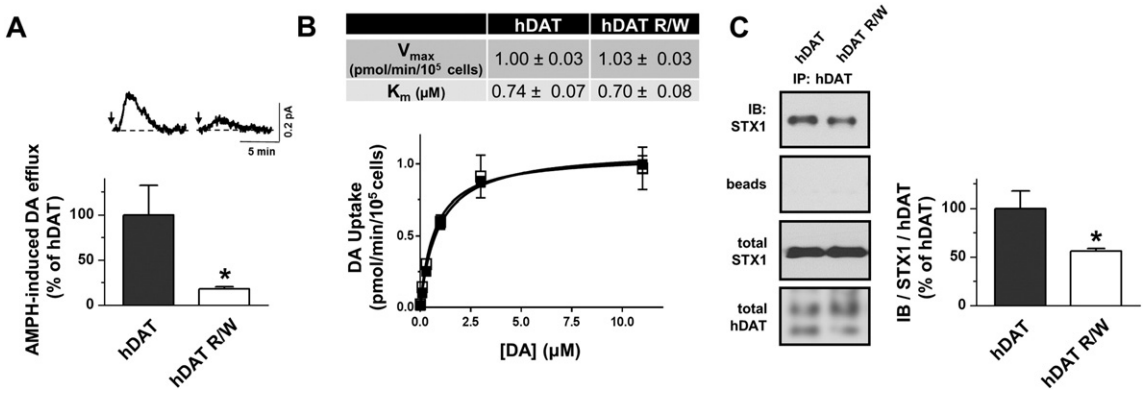

Fig. 3. hDAT R to W missense variant has decreased STX1 association, reduced reverse transport of DA, but normal DA uptake: (A) Top: representative AMPH-induced DA efflux recorded from hDAT or hDAT R/W cells expressing STX1. Arrows indicate application of 10 μM AMPH. Bottom: quantitation of AMPH-induced DA efflux. Data are represented as maximal current expressed as percent of the current recorded in hDAT cells (* = $p < 0.05$ by Student's t-test; n = 5). (B) hDAT R/W exhibits normal DA uptake function. Top: kinetic parameters (V_{max} and K_m) for hDAT and hDAT R/W (V_{max}: $p > 0.92$ by Student's t-test; n = 3, in triplicate; K_m: $p > 0.62$ by Student's t-test; n = 3, in triplicate). Bottom: representative plot of [^{3}H]DA uptake kinetics in hDAT (filled squares) and hDAT R/W (empty squares) cells ($p > 0.05$, by two-way ANOVA followed by Bonferroni post-test; in triplicate). (C) Top: hDAT immunoprecipitates from either hDAT or hDAT R/W cells expressing STX1 were immunoblotted for STX1 (top lane). The beads fraction supports the absence of non-specific binding. Third lane shows an immunoblot for total STX1 proteins. Bottom lane shows an immunoblot for total hDAT proteins. Bottom: quantitation of hDAT pull down band intensities normalized to the respective total STX1 and total hDAT; expressed as a percentage hDAT cells (* = $p < 0.05$ by Student's t-test; n = 5).

decreased association of STX1 to hDAT R/W. We immunoprecipitated hDAT and immunoblotted the immunoprecipitates for STX1 (Fig. 3C). The amount of STX1 recovered in the DAT immunoprecipitates was reduced in the hDAT R/W cells compared to the hDAT cells (Fig. 3C, IB: STX1). In the absence of antibody against DAT, no signal was detected for STX1 in the immunoprecipitates (Fig. 3C, beads). The total STX1 and hDAT in the hDAT R/W cells was not decreased with respect to hDAT cells (Fig. 3C, total STX1 and total hDAT). These data demonstrate that the hDAT R/W variant has a reduced STX1/DAT interaction. Quantitation of multiple experiments is shown in the bar graph of Fig. 3C. These data highlight that the ASD-associated hDAT and STX1 variants both impair reverse transport of DA without inhibiting DAT-mediated DA uptake functions.

3.2. STX1 Phosphorylation Regulates STX1/DAT Interaction

STX1 is phosphorylated at Ser14 by the kinase CK2 (Hirling and Scheller, 1996; Foletti et al., 2000), a posttranslational modification involved in the functional regulation of STX1 (Khelashvili et al., 2012; Dubois et al., 2002). Fig. 2A shows that the STX1 R/Q variant has reduced phosphorylation at Ser14. Therefore, we sought to determine the functional consequences of impaired Ser14 phosphorylation. First, we demonstrated that the highly selective ATP/GTP-competitive inhibitor of CK2, 4,5,6,7-tetrabromobenzotriazole (TBB, 10 μM), effectively reduces p-STX1 in hDAT cells. p-STX1 levels were determined either upon TBB treatment or control conditions with a phospho-specific antibody that recognizes phosphorylation of Ser14 (Castillo et al., 2010) (Fig. 4A).

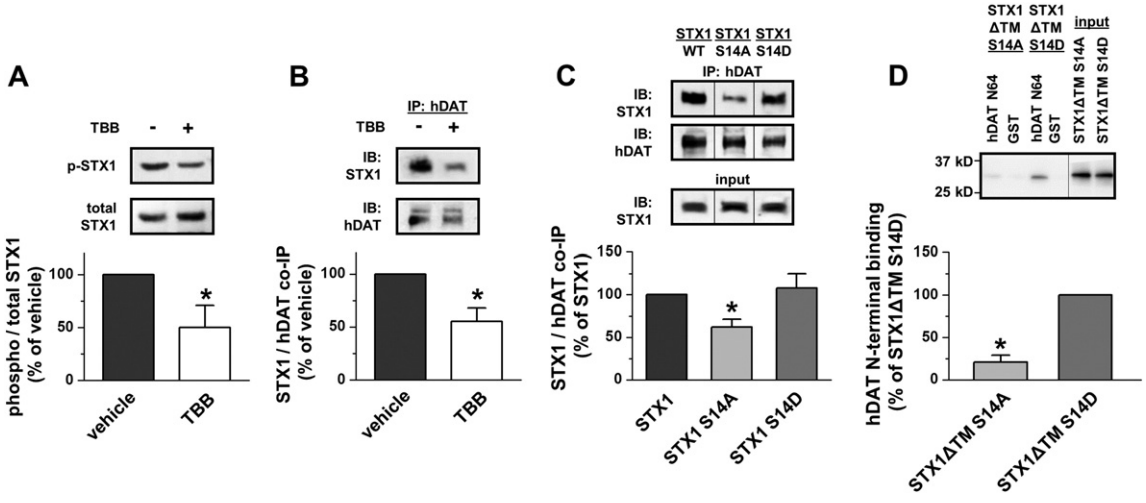

Fig. 4. CK2-mediated phosphorylation of STX1 at S14 promotes STX1/DAT interaction: (A) Stably transfected hDAT cells transfected with STX1 were treated with either vehicle or 10 μM TBB for 20 min. STX1 proteins were immunoblotted for p-STX1 (with a phospho-specific antibody directed against Ser14) and STX1. p-STX1 band densities were normalized to the corresponding total STX1 band densities and expressed as a percentage of vehicle control. CK2 inhibition with TBB significantly decreased the levels of p-STX1 (* = $p < 0.05$ by Student's t-test; n = 4). (B) Stably transfected hDAT cells transfected with STX1 were treated with either vehicle or 10 μM TBB for 20 min. hDAT proteins were immunoprecipitated and immunoblotted for STX1 and DAT. STX1 band densities were normalized to DAT and expressed as a percentage of vehicle control. CK2 inhibition significantly decreased STX1/DAT interaction (* = $p < 0.05$ by Student's t-test; n = 4). (C) Stably transfected hDAT cells were transfected with either STX1, STX1 S14A, or STX1 S14D. hDAT immunoprecipitates were immunoblotted for either STX1 (top band) or hDAT (middle band). Input (bottom band) serves as loading control. All STX1 isoform band densities were normalized to hDAT and expressed as a percentage of STX1. STX1 S14A displays a significantly decreased association with DAT (* = $p < 0.05$ by one-way ANOVA followed by Newman–Keuls Multiple Comparison Test; n = 6). (D) Purified STX1ΔTM peptides (S14A or S14D) were incubated with a GST fusion protein of the first 64 amino acids of the hDAT N-terminus (N64) or with GST alone. The samples were then immunoblotted for STX1. STX1 band densities were expressed as a percentage of STX1ΔTM S14D. STX1ΔTM S14A displays reduced binding to the hDAT N-terminus (* = $p < 0.05$ by Student's t-test; n = 5).

TBB significantly decreases basal levels of p-STX1, demonstrating that CK2 regulates the phosphorylation state of STX1 at Ser14.

Next, we investigated whether STX1 phosphorylation at Ser14 regulates the association of STX1 with the DAT. hDAT cells were treated with either TBB (10 μM for 20 min) or vehicle control, and the cell lysates were immunoprecipitated for DAT and subsequently immunoblotted for STX1. Inhibition of STX1 phosphorylation with TBB reduces STX1/DAT association (Fig. 4B), demonstrating that phosphorylation promotes the STX1/DAT interaction. TBB (10 μM for 20 min) did not change the level of DAT available at the cell surface (hDAT surface expression for TBB exposure was 89.0 ± 12.9% of vehicle control; $p > 0.40$ by Student's t-test; $n = 4$), indicating that the reduced STX1/DAT interaction following CK2 inhibition is not due to DAT trafficking away from the plasma membrane. Collectively, these results are consistent with a coordinated signaling complex whereby phosphorylation of STX1 at Ser14 promotes its association with DAT.

STX1 can be phosphorylated at residues other than Ser14. For example, casein kinase 1 can promote STX1 phosphorylation at Thr21 (Dubois et al., 2002). Therefore, we validated whether the level of phosphorylation of Ser14 alone supports STX1/DAT interactions. We generated STX1 constructs that either prevent Ser14 phosphorylation, by mutating Ser14 to Ala (STX1 S14A), or mimic Ser14 phosphorylation, by mutating Ser14 to Asp (STX1 S14D). We performed immunoprecipitation experiments in hDAT cells transfected with the different STX1 constructs. We observed that the STX1/DAT association is blunted in hDAT cells expressing STX1 S14A as compared to hDAT cells expressing STX1 (Fig. 4C). Furthermore, the pseudo-phosphorylated STX1 S14D exhibits increased interaction with hDAT with respect to STX1 S14A. Thus, phosphorylation of STX1 at Ser14 supports STX1/DAT association. Plasma membrane levels of hDAT, as measured by biotinylation, were not altered by the expression of either STX1 S14A or STX1 S14D when compared to STX1 (STX1 S14A: hDAT surface expression was 101 ± 39% and STX1 S14D: hDAT surface expression was 88 ± 16% relative to hDAT cells expressing STX1; $p > 0.89$ by one-way ANOVA; $n = 5–6$).

To determine whether Ser14 phosphorylation regulates the direct association between STX1 and DAT, we used an in vitro GST pull-down assay modified from Binda et al. (2008), which previously demonstrated that the hDAT N-terminus directly interacts with STX1 (Binda et al., 2008). GST hDAT N-terminal fusion proteins (hDAT N64, see the Materials and Methods section) were used to pull down recombinant soluble constructs of STX1 lacking the transmembrane domain (STX1ΔTM) with Ser14 mutated to Ala (STX1ΔTM S14A) or Asp (STX1ΔTM S14D) (Fig. 4D). hDAT N64 robustly pulled down STX1ΔTM S14D. However, hDAT N64 pull down of STX1ΔTM S14A was dramatically blunted. GST alone did not pull down either STX1ΔTM construct. Quantitative analysis of band densities in Fig. 4D demonstrates that the STX1ΔTM S14A peptide exhibits a significantly reduced direct association with the DAT N-terminus relative to the STX1ΔTM S14D peptide. Input bands show that the STX1ΔTM constructs were of expected size and exhibited minimal degradation. These data further support the notion that STX1 phosphorylation at Ser14 is a key regulator of the dynamic, direct interaction between STX1 and DAT.

3.3. STX1 Phosphorylation Supports Reverse Transport of DA

Fig. 2B shows that the STX1 R/Q variant promotes a reduction in DA efflux. Therefore, it is possible that the CK2-mediated phosphorylation of STX1 at Ser14 support reverse transport of DA. We first determined whether AMPH causes an increase in STX1 phosphorylation. To test this, p-STX1 levels were measured in hDAT cells transfected with STX1 and treated either with vehicle, AMPH, or AMPH in the presence of TBB (Fig. 5A). AMPH treatment increased the level of p-STX1 with respect to vehicle control. Pre-treatment of cells with TBB (10 μM for 20 min) prevented the AMPH-induced phosphorylation of STX1 at Ser14, demonstrating that AMPH induces phosphorylation of STX1 in a CK2-dependent manner. Quantitation of the band density of p-STX1, normalized to total STX1 and expressed as a percent of control is shown in Fig. 5A (bottom).

These findings implicate CK2 and phosphorylation of STX1 at Ser14 as possible novel molecular mediators of reverse transport of DA. Thus, we investigated the role of CK2 function and STX1 phosphorylation at Ser14 in AMPH-induced DA efflux. DA efflux was quantified by amperometry in hDAT cells expressing STX1 under control conditions or pharmacological inhibition of CK2 with TBB (10 μM for 20 min). TBB reduced AMPH-induced DA efflux as compared to vehicle control treated cells (Fig. 5B). These data support our hypothesis that STX1 phosphorylation at Ser14 regulates reverse transport of DA. To further test this hypothesis, we determined if the ability of TBB to regulate DA efflux is altered by preventing or mimicking phosphorylation of STX1. We expressed STX1 S14A or STX1 S14D constructs in hDAT cells and measured AMPH-induced DA efflux in the presence or absence of TBB. In hDAT cells expressing STX1 S14A, AMPH-induced DA efflux was not sensitive to pharmacological inhibition of CK2, and the absolute DA efflux in vehicle control was comparable to hDAT cells expressing STX1 that were TBB treated (Fig. 5C, compare to Fig. 5B TBB treated). Further, in hDAT cells expressing STX1 S14D, AMPH-induced DA efflux was also not sensitive to TBB. However, the absolute DA efflux in the presence of TBB was comparable to vehicle treated hDAT cells expressing STX1 (Fig. 5D, compare to Fig. 5B vehicle treated). These results demonstrate that preventing STX1 phosphorylation (STX1 S14A) parallels pharmacological inhibition of CK2, and mimicking STX1 phosphorylation (STX1 S14D) obscures the ability of TBB to inhibit DA efflux. It also points to the phosphorylation state of STX1 at Ser14 as a determining factor in the magnitude of reverse transport of DA, further supporting our hypothesis that the STX1 R/Q variant alters DA neurotransmission via reduced phosphorylation.

Cultured catecholamine neurons from the superior cervical ganglion (SCG) have large presynaptic boutons that are amenable to imaging approaches, allowing us to determine whether AMPH drives STX1 phosphorylation at these release sites. SCG neurons natively express the NET, which has 66% amino acid sequence homology with the DAT, as well as the accompanying catecholamine presynaptic machinery (Matthies et al., 2009). Here, we utilized confocal imaging of SCG presynaptic boutons coupled with immunofluorescence to reveal the presence of endogenous p-STX1, closely localized to the NET (Supp. Fig. 2A). Consistent with our findings in hDAT cells (see Fig. 5A), AMPH treatment (10 μM for 20 min) enhances STX1 phosphorylation at Ser14 in SCG presynaptic terminals (Supp. Fig. 2B). SCG cultured neurons also express endogenous CK2α (Supp. Fig. 2C). Lastly and notably, in mouse striatal slices, there is a similar profile of endogenous STX1 and p-STX1 expression. (Supp. Fig. 2D). These data present SCG neurons as a biologically relevant preparation in which to observe the functional role of STX1 in reverse transport of DA.

3.4. STX1 Phosphorylation Regulates Reverse Transport of DA at Neuronal Release Sites

Next, we explored the role of STX1 phosphorylation in DAT-mediated reverse transport of DA at the level of the SCG presynaptic boutons. Since SCG neurons do not natively express DAT, we used neurons cultured from NET knockout mice and transiently transfected with hDAT labeled with a GFP tag (Fig. 6A, inset). GFP fluorescence was used to identify neurons positive for hDAT expression. AMPH-induced DA efflux was recorded with amperometry from individual synaptic boutons (Fig. 6A). This DA efflux was cocaine sensitive, indicating its DAT dependence (data not shown). TBB (10 μM for 20 min) reduced AMPH-induced DA release as compared to vehicle control (Fig. 6A). These data demonstrate, at the level of a single bouton, that CK2 function and STX1 phosphorylation are critical mediators of AMPH-induced DAT-mediated DA release.

We then determined the importance of STX1 for reverse transport of DA in ex vivo preparations. In mouse striatal slices, pre-incubation in

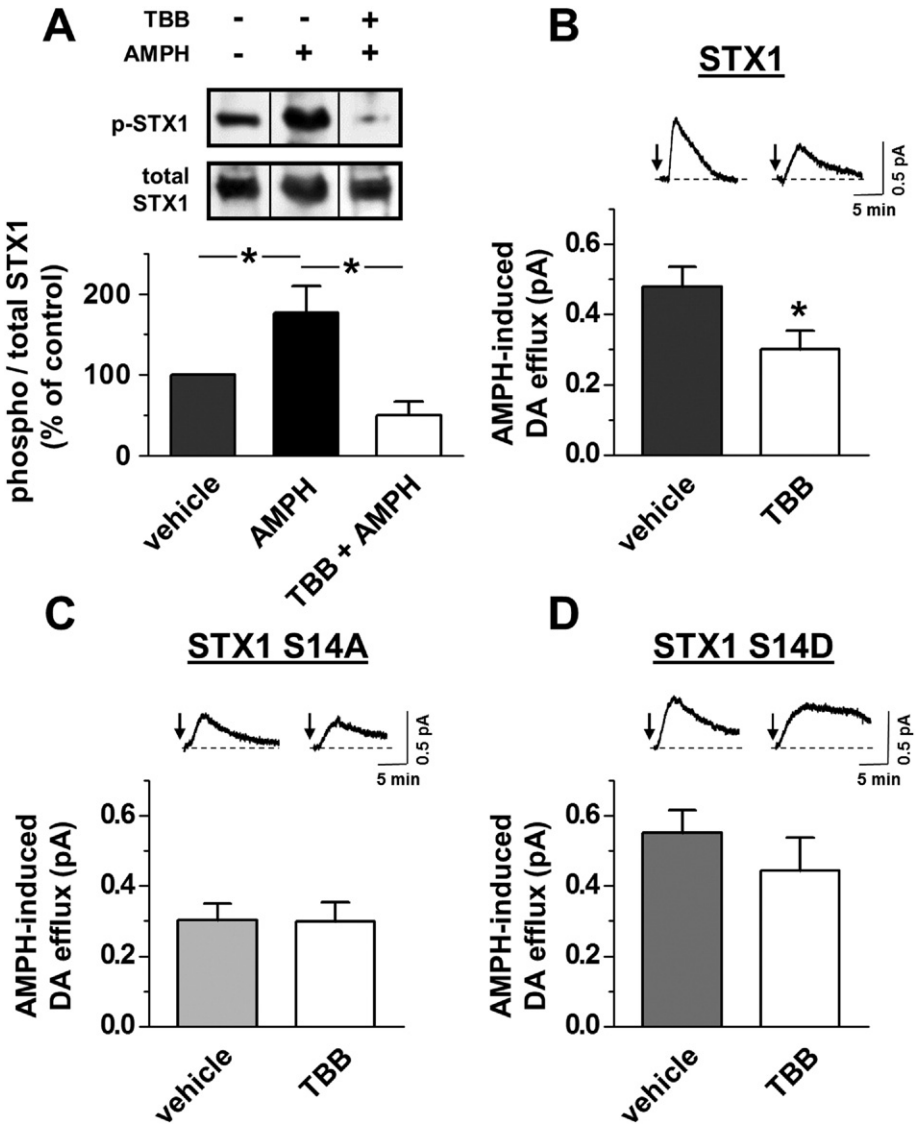

Fig. 5. STX1 phosphorylation promotes reverse transport of DA: (A) Top: stably transfected hDAT cells expressing STX1 were treated with either vehicle or 10 μM TBB for 20 min. This was followed by an additional treatment with vehicle or 10 μM AMPH for 15 min. STX1 immunoprecipitates were immunoblotted for either p-STX1 (Ser14) or STX1. Bottom: the immunoprecipitated band densities were quantified, normalized to the corresponding density of total precipitated STX1, and expressed as a percentage of vehicle control (* = $p < 0.05$ by one-way ANOVA followed by Newman–Keuls Multiple Comparison Test; n = 3). (B) Representative AMPH-induced DA efflux recorded from stably transfected hDAT cells expressing STX1 treated with either vehicle or 10 μM TBB for 20 min just before the amperometric recordings. Arrows indicate application of 10 μM AMPH. Bottom: quantitation of AMPH-induced DA efflux. Data are represented as maximal oxidative current (* = $p < 0.05$ by Student's t-test; n = 5). (C) Representative AMPH-induced amperometric currents recorded from stably transfected hDAT cells expressing STX1 S14A treated with either vehicle or 10 μM TBB for 20 min. Arrows indicate application of 10 μM AMPH. Bottom: quantitation of maximal oxidative current ($p > 0.05$ by Student's t-test; n = 4–7). (D) Representative AMPH-induced amperometric currents recorded from stably transfected hDAT cells expressing STX1 S14D treated with either vehicle or 10 μM TBB for 20 min. Arrows indicate application of 10 μM AMPH. Bottom: quantitation of AMPH-induced DA efflux. Data are represented as maximal oxidative current ($p > 0.05$ by Student's t-test; n = 6).

botulinum toxin serotype C (BoNT/C, 100 nM for 60 min), a protein known to cleave STX1, inhibits AMPH-induced DA efflux as measured by high speed chronoamperometry (Fig. 6B). Importantly, this BoNT/C pre-incubation paradigm was not effective in significantly altering DA uptake (Fig. 6C). These data demonstrate the pivotal role of STX1 in supporting DA efflux without altering forward transport of DA in brain tissues.

3.5. STX1 Phosphorylation and STX1/DAT Association Regulates Dopaminergic Behaviors

In adult *Drosophila* males, we developed locomotor assays for an in vivo examination of DAT-mediated reverse transport of DA and the impact of ASD variants on this transport process. First, we explored how impairments in STX1 phosphorylation, which affects STX1/DAT associations, regulate DA-associated behaviors. In *Drosophila*, locomotion requires functional DA neurotransmission (Hamilton et al., 2013, 2014; Pizzo et al., 2013). To probe for changes in locomotion, adult males were fed a sucrose solution containing either AMPH (1 mM) or vehicle. We observed that AMPH significantly stimulated locomotion in wild-type (WT) *Drosophila* (Fig. 7A). However, AMPH did not significantly increase locomotion in flies lacking dDAT (DAT KO) (Kume et al., 2005), indicating that AMPH-induced locomotion is a DAT-dependent behavior (Fig. 7A). These data strongly support this assay as a model to test the multiple functions of DAT in vivo.

CK2 function promotes STX1 phosphorylation at Ser14, STX1/DAT interaction, and reverse transport of DA. Thus, to probe the behavioral significance of impaired STX1 phosphorylation at Ser14 and STX1/DAT interaction, we evaluated whether inhibited CK2 function alters AMPH-induced locomotion. We expressed a dominant negative form

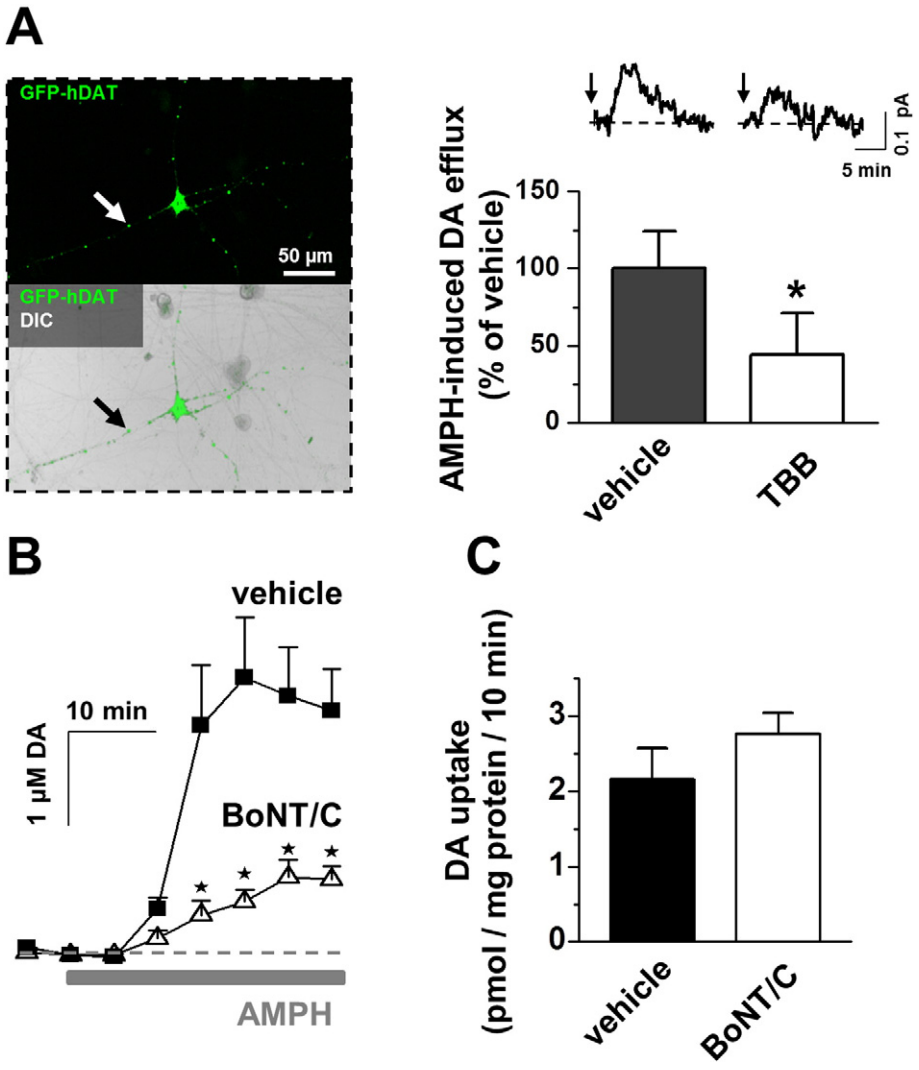

Fig. 6. Inhibition of STX1 phosphorylation or cleavage of STX1 inhibits DA efflux but not uptake: (A) *Inset*: Image of a single GFP-hDAT transfected SCG neuron; arrows indicate the site of amperometric recording (i.e. the presynaptic bouton). Top: representative AMPH-induced amperometric currents recorded from a single presynaptic bouton of SCG neurons expressing GFP-hDAT after treatment with either vehicle or 10 μM TBB for 20 min. Bottom: quantitation of the maximal oxidative current normalized to vehicle treatment (* = $p < 0.05$ by Student's t-test; n = 5). (B) AMPH (10 μM)-induced DA efflux recorded in mouse striatal slices preincubated (1 h) either with vehicle or BoNT/C (100 nM) (* = $p < 0.05$ by two-way ANOVA; n = 6). (C) [^{3}H]DA uptake measure in striatal slices receiving identical treatment as in panel (c) ($p > 0.05$ by Student's t-test; n = 4).

of CK2 (CK2DN) in flies by using the Gal4/UAS system to express a single copy CK2DN in a WT background, selectively in DA neurons. We compared the AMPH-induced behavioral responses of flies expressing CK2DN to WT flies. AMPH did not significantly increase locomotor activity in flies expressing dominant negative CK2 mutant (Fig. 7B). Furthermore, vehicle treatment did not modify locomotion of flies expressing CK2DN with respect to WT flies, suggesting that extracellular DA level did not change under basal conditions. Consistent with this, CK2 inhibition by TBB treatment (10 μM for 15 min) did not alter DA uptake in intact *Drosophila* brains (Fig. 7B, inset). Importantly, brains obtained from dDAT KO flies show robustly reduced DA uptake, demonstrating the DAT dependence of DA uptake in our newly developed uptake assay. Collectively, these data point to CK2 activity, STX1 phosphorylation at Ser14, and STX1/DAT association as critical mediators of reverse transport of DA and associated behaviors.

Next, we explored how the ASD-associated hDAT R/W variant that impairs STX1/DAT association affects DA-dependent behaviors in our *Drosophila* model system. We expressed hDAT or hDAT R/W in DA neurons of dDAT KO flies as described above. We fed male *Drosophila* a sucrose solution containing either AMPH (1 mM) or vehicle and quantified locomotion in 30-minute intervals. AMPH exposure induced a significantly smaller increase in locomotion in hDAT R/W expressing flies as compared to hDAT expressing flies (Fig. 7C, compare hDAT + AMPH versus hDAT R/W + AMPH). These data are consistent with the reduced ability of AMPH to cause DA efflux in hDAT R/W expressing cells. Basal locomotion of flies expressing hDAT R/W did not significantly differ from hDAT expressing flies.

4. Discussion

Alterations in DA neurotransmission have been identified in several neuropsychiatric disorders, including ASD (Nguyen et al., 2014; Cousins et al., 2009; Seeman et al., 1990; Volkow et al., 2007). Recently, we demonstrated that an ASD-associated hDAT de novo variant displays dramatically altered DAT function, including constitutive reverse transport of DA, which leads to hyperlocomotion (Hamilton et al., 2013). Thus, we hypothesized that novel DAT variants (or variant in the genes known to regulate the DAT) that affect DA neurotransmission might contribute to the pathology and/or complications of ASD. We identify and describe two independent gene variants that converge mechanistically to disrupt DAT function and associated behaviors, with distinct mechanisms regulating either STX1 phosphorylation or STX1/DAT interaction.

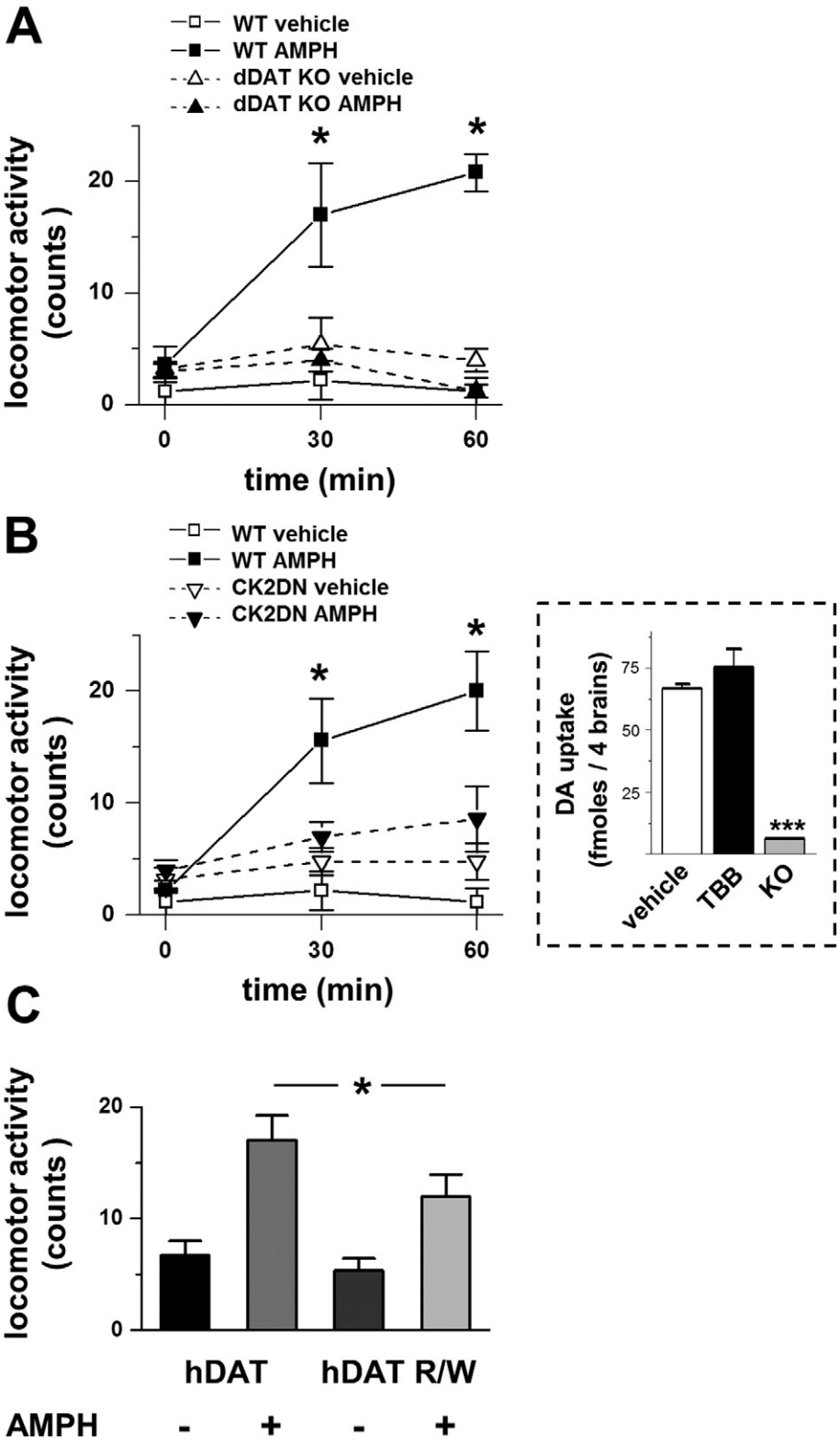

Fig. 7. STX1 phosphorylation regulates AMPH-induced behaviors: (A) DAT knockout (KO) flies demonstrate that AMPH-induced locomotor behavior is DAT-dependent. Locomotor activity in response to vehicle (open symbols) or (1 mM) AMPH (filled symbols) in either wild-type (WT) (squares) or in DAT KO flies (triangles). WT flies exhibit a significant AMPH-induced increase in locomotion while DAT KO flies do not exhibit this significant increase (* = $p < 0.05$ for vehicle vs AMPH, two-way ANOVA followed by Bonferroni post-test; n = 5). (B) *Drosophila* were generated expressing a dominant-negative (DN) version of CK2α expressed specifically in dopaminergic neurons. Locomotor activity in response to vehicle (open symbols) or AMPH (filled symbols) in either wild-type (WT) (squares) or in CK2 dominant negative flies (CK2DN) (triangles). WT flies exhibit a significant increase in AMPH-induced locomotion while CK2DN flies do not (* = $p < 0.05$ for vehicle vs AMPH, two-way ANOVA followed by Bonferroni post-test; n = 5). *Inset*: DA uptake in intact fly brains in the presence of 10 μM TBB or vehicle. The absence of uptake in the dDAT KO fly brains shows the dependence of DA uptake on the dDAT (*** = $p < 0.0001$ by one-way ANOVA followed by Newman–Keuls Multiple Comparison Test; n = 3). (C) hDAT R/W expressing flies have blunted locomotor responses to AMPH. Changes in locomotion were determined upon AMPH or vehicle exposure over 30 min and calculated as beam crosses (counts). AMPH (1 mM) caused a significant increase in locomotion in both hDAT flies ($p < 0.001$ by one-way ANOVA followed by Newman–Keuls Multiple Comparison Test; n = 24) and hDAT R/W flies ($p < 0.05$ by one-way ANOVA followed by Newman–Keuls Multiple Comparison Test; n = 24). However, in hDAT R/W flies, AMPH exposure led to a reduced increase in locomotion than in hDAT flies (* = $p < 0.05$ by one-way ANOVA followed by Newman–Keuls Multiple Comparison Test; n = 24).

We found that the STX1 R/Q variant has decreased phosphorylation of Ser14, a key residue involved in the functional regulation of STX1 (Khelashvili et al., 2012; Dubois et al., 2002). STX1 in this hypo-phosphorylated state fails to support DAT-mediated reverse transport of DA without inhibiting DA uptake function. Interestingly, in hDAT cells expressing STX1 R/Q, we observe a significantly increased V_{max} of DA uptake. In parallel experiments in mouse striatal slices, cleaving STX1 with BoNT/C promotes a decrease in reverse transport of DA with a trend towards increased DA uptake. These data suggest that STX1 function asymmetrically regulates reverse transport of DA and DA uptake. Therefore, to define how hypo-phosphorylation of STX1 R/Q impairs DA reverse transport, we studied the regulatory effects of CK2 function on DA efflux.

CK2 phosphorylates STX1 at Ser14 to regulate STX1 function and protein interactions (Hirling and Scheller, 1996; Foletti et al., 2000; Dubois et al., 2002). Here, we discovered that CK2-mediated phosphorylation of STX1 at Ser14 increases the direct association between STX1 and the hDAT N-terminus. Consistently, pharmacological inhibition of CK2 strongly reduces reverse transport of DA without altering DA uptake. Thus, CK2 is a key player involved in DA efflux. It is possible that this mechanism is important in a broader array of DA-associated neuropsychiatric disorders, since the expression of CK2, as well as the phosphorylation state of STX1 at Ser14, is decreased in post-mortem brain tissue from patients with schizophrenia (Castillo et al., 2010; Aksenova et al., 1991). To have a more complete understanding of how genetic variants within the DA network discovered in ASD patients alter behaviors, we translated our molecular discoveries in vivo. First, we inhibited CK2 function by selectively expressing CK2DN specifically in DA neurons of WT flies. *Drosophila* expressing CK2DN exhibited a robust reduction in AMPH-induced hyperlocomotion as compared to WT flies. These data underscore the importance of CK2 function and STX1 phosphorylation in regulating behaviors sustained by reverse transport of DA. Interestingly, inhibiting CK2 function did not regulate basal locomotion or DA uptake in intact *Drosophila* brains.

Parallel to STX1 R/Q, we found that the hDAT R/W variant displays inhibited reverse transport of DA without impairments in uptake function. It is important to note that CK2 function, in addition to phosphorylating STX1 at Ser14, also promotes STX1/DAT interactions. Here, we show that hDAT R/W has reduced association with STX1, resulting in reduced reverse transport of DA and DA-related behaviors. *Drosophila* expressing hDAT R/W selectively in DA neurons demonstrate reduced sensitivity to the psychomotor effects of AMPH. Interestingly, basal locomotion remained unaltered in hDAT R/W flies, indicating normal DAT-mediated DA clearance as supported by our uptake data. These data suggest that the phosphorylation state of STX1 at Ser14 and STX1/DAT interaction asymmetrically regulate reverse transport of DA and DAT-mediated uptake.

Mounting evidence demonstrates that reverse transport of DA and associated behaviors can be promoted by changes in the association between the N-terminus of DAT and STX1 (Binda et al., 2008). Additionally, it has been suggested that reverse transport of DA might participate in shaping DA neurotransmission (Leviel, 2011). Here, we used AMPH as a tool to induce reverse transport of DA to determine whether ASD-associated variants disrupt this event. We show that AMPH promotes phosphorylation of STX1 at Ser14 and, as a consequence, STX1/DAT interaction to cause reverse transport of DA. Therefore, we felt that it was important to demonstrate these discoveries at the level of a single active site, the SCG bouton.

Several ASD-associated hDAT variants have now been found to impact reverse transport of DA. The STX1 R/Q variant reported here ablates AMPH-induced efflux similarly to hDAT R/W. Interestingly, two other variants were previously found to cause dysregulation of DA efflux, including a de novo DAT T356M variant and the recurrent DAT A559V variant seen in two boys with ASD, as well as in individuals with bipolar disorder and ADHD. These findings demonstrate diverging mechanisms by which reverse transport of DA can be disrupted. They align with other examples of neurodevelopmental risk emerging from genetic variants causing opposite effects on gene expression or signaling cascades (Sanders et al., 2011; Cook et al., 1997).

Here, we characterize two independent autism-associated variants in the genes that encode STX1 and the DAT. We demonstrate that each variant dramatically alters DAT function. We identify molecular mechanisms that converge to inhibit reverse transport of DA and DA-associated behaviors. The physiological importance of reverse transport of DA has only recently emerged and remains incompletely understood. However, defining the molecular identity and the impact of these variants on DA efflux may further shape our understanding of the etiology of ASD. Therefore, large genotyping studies aimed at uncovering other variants of the hDAT and STX1A genes in ASD cases and matched controls would be worthwhile.

Funding

This work was supported by the NSF fellowship DGE0909667 (P.J.H.) and the NIH fellowship DA 035535 (P.J.H.), NIH grants DA038058 and DA012408 (A.G. & U.G.) as well as by the Danish Council for Independent Research | Medical Sciences) (U.G.). N.G.C. was supported by the Training Program in Ion Channel and Transporter Biology (NIH T32NS007491). The funding sources had no role in the writing or submission of the manuscript. We have not been paid to write the article by any company or agency.

Competing Interests

JV has consulted with Roche, Novartis, and SynapDx and has received research funding from Roche, Novartis, SynapDx, Seaside Therapeutics, Forest, and Sunovion for unrelated work.

Authors' Contributions

Author contributions: E.C., P.J.H., A.N.B., A.S., N.G.C., C.S., T.F.A., U.G., J.V., J.S.S., P.G.U., K.E., H.J.G.M., and A.G. designed research; E.C., P.J.H., A.N.B., A.S., N.G.C., C.S., and T.F.A. performed research; and E.C., P.J.H., A.N.B., A.S., N.G.C., C.S., T.F.A., U.G., J.V., J.S.S., P.G.U., K.E., H.J.G.M., and A.G. wrote the paper.

Abbreviations

5-hydroxytryptamine, DA dopamine
hDAT human dopamine transporter
AMPH amphetamine
STX1 syntaxin 1B

Acknowledgments

We thank Nicole Bibus Christianson and Amanda Poe for excellent technical assistance.

Appendix A. Supplementary data

Supplementary data to this article can be found online at http://dx.doi.org/10.1016/j.ebiom.2015.01.007.

References

Rowberry, J., Macari, S., Chen, G., et al., 2015. Screening for autism spectrum disorders in 12-month-old high-risk siblings by parental report. J. Autism Dev. Disord. 45 (1), 221–229.

Wolff, J.J., Botteron, K.N., Dager, S.R., et al., 2014. Longitudinal patterns of repetitive behavior in toddlers with autism. J. Child Psychol. Psychiatry 55 (8), 945–953.

Langen, M., Bos, D., Noordermeer, S.D., Nederveen, H., van Engeland, H., Durston, S., 2014. Changes in the development of striatum are involved in repetitive behavior in autism. Biol. Psychiatry 76 (5), 405–411.

Langen, M., Durston, S., Staal, W.G., Palmen, S.J., van Engeland, H., 2007. Caudate nucleus is enlarged in high-functioning medication-naive subjects with autism. Biol. Psychiatry 62 (3), 262–266.
Langen, M., Schnack, H.G., Nederveen, H., et al., 2009. Changes in the developmental trajectories of striatum in autism. Biol. Psychiatry 66 (4), 327–333.
Hollander, E., Anagnostou, E., Chaplin, W., et al., 2005. Striatal volume on magnetic resonance imaging and repetitive behaviors in autism. Biol. Psychiatry 58 (3), 226–232.
Dichter, G.S., Richey, J.A., Rittenberg, A.M., Sabatino, A., Bodfish, J.W., 2012. Reward circuitry function in autism during face anticipation and outcomes. J. Autism Dev. Disord. 42 (2), 147–160.
Damiano, C.R., Aloi, J., Treadway, M., Bodfish, J.W., Dichter, G.S., 2012. Adults with autism spectrum disorders exhibit decreased sensitivity to reward parameters when making effort-based decisions. J. Neurodev. Disord. 4 (1), 13.
Lin, A., Rangel, A., Adolphs, R., 2012. Impaired learning of social compared to monetary rewards in autism. Front. Neurosci. 6, 143.
Kohls, G., Perino, M.T., Taylor, J.M., et al., 2013. The nucleus accumbens is involved in both the pursuit of social reward and the avoidance of social punishment. Neuropsychologia 51 (11), 2062–2069.
Kohls, G., Thonessen, H., Bartley, G.K., et al., 2014. Differentiating neural reward responsiveness in autism versus ADHD. Dev. Cogn. Neurosci. 10C, 104–116.
Zald, D.H., Boileau, I., El-Dearedy, W., et al., 2004. Dopamine transmission in the human striatum during monetary reward tasks. J. Neurosci. 24 (17), 4105–4112.
Howe, M.W., Tierney, P.L., Sandberg, S.G., Phillips, P.E., Graybiel, A.M., 2013. Prolonged dopamine signalling in striatum signals proximity and value of distant rewards. Nature 500 (7464), 575–579.
Howe, M.W., Atallah, H.E., McCool, A., Gibson, D.J., Graybiel, A.M., 2011. Habit learning is associated with major shifts in frequencies of oscillatory activity and synchronized spike firing in striatum. Proc. Natl. Acad. Sci. U. S. A. 108 (40), 16801–16806.
Fasano, A., Petrovic, I., 2010. Insights into pathophysiology of punding reveal possible treatment strategies. Mol. Psychiatry 15 (6), 560–573.
Kristensen, A.S., Andersen, J., Jorgensen, T.N., et al., 2011. SLC6 neurotransmitter transporters: structure, function, and regulation. Pharmacol. Rev. 63 (3), 585–640.
Binda, F., Dipace, C., Bowton, E., et al., 2008. Syntaxin 1A interaction with the dopamine transporter promotes amphetamine-induced dopamine efflux. Mol. Pharmacol. 74 (4), 1101–1108.
Quick, M.W., 2006. The role of SNARE proteins in trafficking and function of neurotransmitter transporters. Handb. Exp. Pharmacol. 175, 181–196.
Quick, M.W., 2003. Regulating the conducting states of a mammalian serotonin transporter. Neuron 40 (3), 537–549.
Quick, M.W., 2002. Role of syntaxin 1A on serotonin transporter expression in developing thalamocortical neurons. Int. J. Dev. Neurosci. 20 (3–5), 219–224.
Dipace, C., Sung, U., Binda, F., Blakely, R.D., Galli, A., 2007. Amphetamine induces a calcium/calmodulin-dependent protein kinase II-dependent reduction in norepinephrine transporter surface expression linked to changes in syntaxin 1A/transporter complexes. Mol. Pharmacol. 71 (1), 230–239.
Nakamura, K., Anitha, A., Yamada, K., et al., 2008. Genetic and expression analyses reveal elevated expression of syntaxin 1A (STX1A) in high functioning autism. Int. J. Neuropsychopharmacol. 11 (8), 1073–1084.
Nakamura, K., Iwata, Y., Anitha, A., et al., 2011. Replication study of Japanese cohorts supports the role of STX1A in autism susceptibility. Prog. Neuropsychopharmacol. Biol. Psychiatry 35 (2), 454–458.
Durdiakova, J., Warrier, V., Banerjee-Basu, S., Baron-Cohen, S., Chakrabarti, B., 2014. STX1A and Asperger syndrome: a replication study. Mol. Autism 5 (1), 14.
Hamilton, P.J., Campbell, N.G., Sharma, S., et al., 2013. De novo mutation in the dopamine transporter gene associates dopamine dysfunction with autism spectrum disorder. Mol. Psychiatry 18 (12), 1315–1323.
Bowton, E., Saunders, C., Reddy, I.A., et al., 2014. SLC6A3 coding variant Ala559Val found in two autism probands alters dopamine transporter function and trafficking. Transl. Psychiatry 4, e464.
Hettinger, J.A., Liu, X., Hudson, M.L., et al., 2012. DRD2 and PPP1R1B (DARPP-32) polymorphisms independently confer increased risk for autism spectrum disorders and additively predict affected status in male-only affected sib-pair families. Behav. Brain Funct. 8, 19.
Qian, Y., Chen, M., Forssberg, H., Diaz, Heijtz R., 2013. Genetic variation in dopamine-related gene expression influences motor skill learning in mice. Genes Brain Behav. 12 (6), 604–614.
Reiersen, A.M., Todorov, A.A., 2011. Association between DRD4 genotype and autistic symptoms in DSM-IV ADHD. J. Can. Acad. Child Adolesc. Psychiatry 20 (1), 15–21.
Yoo, H.J., Cho, I.H., Park, M., Yang, S.Y., Kim, S.A., 2013. Association of the catechol-o-methyltransferase gene polymorphisms with Korean autism spectrum disorders. J. Korean Med. Sci. 28 (9), 1403–1406.
Nguyen, M., Roth, A., Kyzar, E.J., et al., 2014. Decoding the contribution of dopaminergic genes and pathways to autism spectrum disorder (ASD). Neurochem. Int. 66, 15–26.
Leviel, V., 2011. Dopamine release mediated by the dopamine transporter, facts and consequences. J. Neurochem. 118 (4), 475–489.
Neale, B.M., Kou, Y., Liu, L., et al., 2012. Patterns and rates of exonic de novo mutations in autism spectrum disorders. Nature 485 (7397), 242–245.
Lim, E.T., Raychaudhuri, S., Sanders, S.J., et al., 2013. Rare complete knockouts in humans: population distribution and significant role in autism spectrum disorders. Neuron 77 (2), 235–242.
Liu, L., Sabo, A., Neale, B.M., et al., 2013. Analysis of rare, exonic variation amongst subjects with autism spectrum disorders and population controls. PLoS Genet. 9 (4), e1003443.
De Rubeis, S., He, X., Goldberg, A.P., et al., 2014. Synaptic, transcriptional and chromatin genes disrupted in autism. Nature 515 (7526), 209–215.
Iossifov, I., O'Roak, B.J., Sanders, S.J., et al., 2014. The contribution of de novo coding mutations to autism spectrum disorder. Nature 515 (7526), 216–221.
Bowton, E., Saunders, C., Erreger, K., et al., 2010. Dysregulation of dopamine transporters via dopamine D2 autoreceptors triggers anomalous dopamine efflux associated with attention-deficit hyperactivity disorder. J. Neurosci. 30 (17), 6048–6057.
Castillo, M.A., Ghose, S., Tamminga, C.A., Ulery-Reynolds, P.G., 2010. Deficits in syntaxin 1 phosphorylation in schizophrenia prefrontal cortex. Biol. Psychiatry 67 (3), 208–216.
Kume, K., Kume, S., Park, S.K., Hirsh, J., Jackson, F.R., 2005. Dopamine is a regulator of arousal in the fruit fly. J. Neurosci. 25 (32), 7377–7384.
Bose, A., Kahali, B., Zhang, S., et al., 2006. Drosophila CK2 regulates lateral-inhibition during eye and bristle development. Mech. Dev. 123 (9), 649–664.
Lin, J.M., Kilman, V.L., Keegan, K., et al., 2002. A role for casein kinase 2alpha in the Drosophila circadian clock. Nature 420 (6917), 816–820.
Rasmussen, T., Skjoth, I.H., Jensen, H.H., Niefind, K., Boldyreff, B., Issinger, O.G., 2005. Biochemical characterization of the recombinant human Drosophila homologues Timekeeper and Andante involved in the Drosophila circadian oscillator. Mol. Cell. Biochem. 274 (1–2), 151–161.
Hirling, H., Scheller, R.H., 1996. Phosphorylation of synaptic vesicle proteins: modulation of the alpha SNAP interaction with the core complex. Proc. Natl. Acad. Sci. U. S. A. 93 (21), 11945–11949.
Foletti, D.L., Lin, R., Finley, M.A., Scheller, R.H., 2000. Phosphorylated syntaxin 1 is localized to discrete domains along a subset of axons. J. Neurosci. 20 (12), 4535–4544.
Khelashvili, G., Galli, A., Weinstein, H., 2012. Phosphatidylinositol 4,5-biphosphate (PIP(2)) lipids regulate the phosphorylation of syntaxin N-terminus by modulating both its position and local structure. Biochemistry 51 (39), 7685–7698.
Dubois, T., Kerai, P., Learmonth, M., Cronshaw, A., Aitken, A., 2002. Identification of syntaxin-1A sites of phosphorylation by casein kinase I and casein kinase II. Eur. J. Biochem. 269 (3), 909–914.
Matthies, H.J., Han, Q., Shields, A., et al., 2009. Subcellular localization of the antidepressant-sensitive norepinephrine transporter. BMC Neurosci. 10, 65.
Pizzo, A.B., Karam, C.S., Zhang, Y., et al., 2013. The membrane raft protein Flotillin-1 is essential in dopamine neurons for amphetamine-induced behavior in Drosophila. Mol. Psychiatry 18 (7), 824–833.
Hamilton, P.J., Belovich, A.N., Khelashvili, G., et al., 2014. PIP2 regulates psychostimulant behaviors through its interaction with a membrane protein. Nat. Chem. Biol. 10 (7), 582–589.
Cousins, D.A., Butts, K., Young, A.H., 2009. The role of dopamine in bipolar disorder. Bipolar Disord. 11 (8), 787–806.
Seeman, P., Niznik, H.B., Guan, H.C., 1990. Elevation of dopamine D2 receptors in schizophrenia is underestimated by radioactive raclopride. Arch. Gen. Psychiatry 47 (12), 1170–1172.
Volkow, N.D., Fowler, J.S., Wang, G.J., Swanson, J.M., Telang, F., 2007. Dopamine in drug abuse and addiction: results of imaging studies and treatment implications. Arch. Neurol. 64 (11), 1575–1579.
Aksenova, M.V., Burbaeva, G.S., Kandror, K.V., Kapkov, D.V., Stepanov, A.S., 1991. The decreased level of casein kinase 2 in brain cortex of schizophrenic and Alzheimer's disease patients. FEBS Lett. 279 (1), 55–57.
Sanders, S.J., Ercan-Sencicek, A.G., Hus, V., et al., 2011. Multiple recurrent de novo CNVs, including duplications of the 7q11.23 Williams syndrome region, are strongly associated with autism. Neuron 70 (5), 863–885.
Cook Jr., E.H., Lindgren, V., Leventhal, B.L., et al., 1997. Autism or atypical autism in maternally but not paternally derived proximal 15q duplication. Am. J. Hum. Genet. 60 (4), 928–934.